Journal of Chromatography A, 1217 (2010) 6077–6084

Contents lists available at ScienceDirect

Journal of Chromatography A

journal homepage: www.elsevier.com/locate/chroma

Hydrodynamic chromatography of polystyrene microparticles in micropillar array columns

Jeff Op de Beeck[a], Wim De Malsche[a], Joris Vangelooven[a], Han Gardeniers[b], Gert Desmet[a,*]

[a] Vrije Universiteit Brussel, Department of Chemical Engineering, Pleinlaan 2, 1050 Brussels, Belgium
[b] Research Programme Mesofluidics, MESA+ Research Institute, P.O. Box 217, 7500 AE Enschede, The Netherlands

ARTICLE INFO

Article history:
Received 29 March 2010
Received in revised form 1 July 2010
Accepted 14 July 2010
Available online 21 July 2010

Keywords:
Hydrodynamic chromatography
Size separation
Microparticles
Micropillar array column

ABSTRACT

We report on the possibility to perform HDC in micropillar array columns and the potential advantages of such a system. The HDC performance of a pillar array column with pillar diameter = 5 μm and an interpillar distance of 2.5 μm has been characterized using both a low MW tracer (FITC) and differently sized polystyrene bead samples (100, 200 and 500 nm). The reduced plate height curves that were obtained for the different investigated markers all overlapped very well, and attained a minimum value of about h_{min} = 0.3 (reduction based on the pillar diameter), corresponding to 1.6 μm in absolute value and giving good prospects for high efficiency separations. The obtained reduced retention time values were in fair agreement with that predicted by the Di Marzio and Guttman model for a flow between flat plates, using the minimal interpillar distance as characteristic interplate distance.

1. Introduction

The search for a method that allows a fast and reliable size-dependent separation or characterization of cells, macromolecules and particles remains one of the greatest challenges in today's analytical chemistry. As one of the essential tools in biochemical, biomedical, environmental and industrial applications, this topic has been extensively studied over the last decades resulting in the development of a wide range of techniques. Classical techniques like filtration, centrifugation or sedimentation can be used to separate large analytes. However, when the analytes become smaller or the difference in size becomes smaller, these techniques tend to fail and other techniques which have a higher resolution are recommended.

Next to conventional methods such as size exclusion chromatography (SEC), gel permeation chromatography (GPC) and field flow fractionation (FFF), the concept of hydrodynamic chromatography (HDC) has been proposed in the 1970s as an alternative method to separate analytes based on their size [1]. HDC has the potential to provide a faster and more efficient analysis than SEC and GPC, as its speed is not limited by the slow mass transfer process which takes place in the porous particles [2,3]. Because HDC can be performed in any desirable carrier fluid, biological activity of samples can be maintained and consumption of often toxic solvents can be omitted. The HDC principle relies on the size-dependent exclusion from the wall-region in channels which have a Poiseuille-like flow [4]. Due to steric hindrance, large analytes cannot access the low fluid velocity regions near the channel wall, resulting in a larger average velocity as compared to smaller analytes which can access these regions (Fig. 1a and b). Therefore, HDC has the same elution order as seen in GPC, SEC or the steric mode of FFF, with the large analytes eluting first, followed by the smaller ones. FFF is based on the same hydrodynamic principle, but an additional field can be applied in order to obtain a higher resolution [5]. The large family of FFF techniques includes sedimentation, flow, thermal, electrical and other types of FFF which have all been successfully applied for the size characterization of large sized analytes. Although these techniques generally have a higher selectivity as compared to HDC, they are often complicated in handling and manufacturing, limited in choice of carrier fluid or require high electrical power consumption [6–8]. However, HDC in packed-bed columns still has a very poor efficiency as compared to the previously mentioned methods. The high flow resistance of packed-bed columns urges the use of large packing particles that have nonuniform flow-through pores, which in turn have a very detrimental effect on the separation efficiency.

The need for a technique that combines high selectivity and resolution, low sample and solvent consumption and fast analysis time has driven research towards the miniaturization of analytical separation methods [9,10]. The first miniaturization in the field of HDC was done by substituting the packed columns by an open tubular column (microcapillary). Besides significantly improving the resolution, sample and solvent consumption can be reduced drastically. Unfortunately, because of the limited injection

* Corresponding author. Tel.: +32 26293251; fax: +32 26293248.
E-mail address: gedesmet@vub.ac.be (G. Desmet).

0021-9673/$ – see front matter © 2010 Elsevier B.V. All rights reserved.
doi:10.1016/j.chroma.2010.07.031

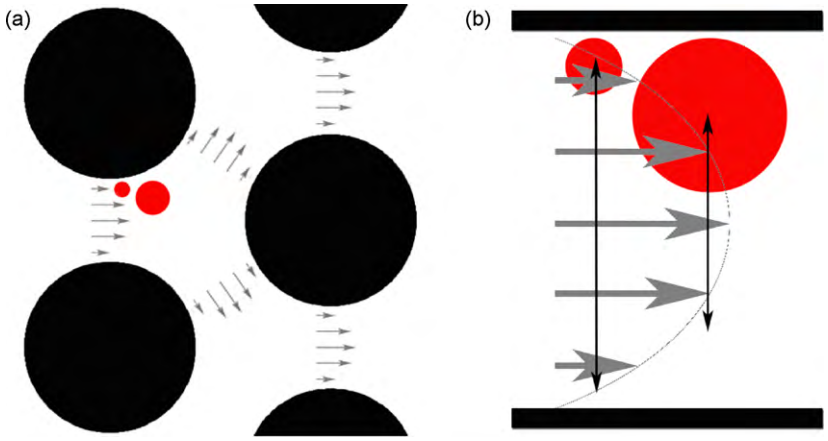

Fig. 1. Principle of HDC in a micropillar array. (a) In narrow channels with a laminar flow, the flow velocity has a parabolic profile. Larger analytes are not able to access the low fluid velocity regions near the wall, whereas smaller will. Therefore the larger ones will move faster. (b) Zoom-in of the interpillar region in (a).

volume and the small dimension of these microcapillaries, detection becomes tedious and very sensitive detection equipment is needed [11,12]. To overcome these limitations, an on-chip HDC system was developed by Chmela et al. [13–15]. On this chip, the channel cross-section uniformity and well defined depth of 1 μm guaranteed a good separation resolution, whereas the large channel width could ensure an adequate injection volume. Although the experimental performance for different fluorescent microparticles and biopolymers was found to be sufficient for an HDC separation, it was still lower than what theory predicted. Visualization of the fluorescent analyte bands in the channel revealed a characteristic deformed peak shape for all analytes. The deformation of the peaks apparently originated from the existence of a nonuniform flow profile across the channel width. This could be explained as follows: due to mechanical and fabrication limitations, the center of the channel has an increased thickness, resulting in an increased flow speed in this region. Besides, the sidewall induced dispersion (sidewall effect) [16] can also be expected to contribute to the deformation of the peak shapes, but this effect could well be hidden in the extra dispersion caused by the former effect.

With the introduction of micropillar array columns in the field of chromatography, it can be expected that even more performant HDC separations will become possible. The advantages of these columns over classical packed-bed columns have already been extensively described for the use of partition- and adsorption chromatography [17–19], but this format is also very promising for HDC separations. Using advanced micromachining, micropillars up to 30 μm high can be etched in a silicon wafer at a submicrometer interpillar distance, and at the same time the channel depth and interpillar distance can be kept constant. Hence, the separation resolution can be maximized by keeping a small radial distance between the micropillars, while the depth and the width of the channel provide the possibility to increase the volumetric capacity. Furthermore, the presence of the micropillars is believed to be advantageous for the separation efficiency in several ways. Since the micropillars provide extra anchor points between the silicon wafer and the pyrex top plate, the channel depth will be constant through the whole column. This eliminates the nonuniform flow profile observed in the on-chip HDC system of Chmela et al. Furthermore, positioning the pillars at a certain distance (the so-called "magical"-wall distance) from the sidewall allows completely eliminating the sidewall effect as shown in the previous work of our group [20,21,16].

The present paper reports on an experimental study of the HDC separation properties of a silicon micropillar column.

2. Experimental

2.1. Channel fabrication

The pillar channel consisted of a 2.5 cm long, 2 mm wide and 12 μm deep channel filled with cylindrical pillars at an interpillar distance of 2.5 μm. The pillars were equilaterally positioned in respect to each other as it was patterned on a photolithographic mask. To fabricate the channels, a 100 mm diameter (100) silicon wafer (p-type, 5–10 Ω cm resistivity) was first thermally (dry) oxidized at 1100 °C until 200 nm silicon oxide was formed (Amtech Tempress Omega Junior). Then, normal wavelength UV photolithography (photoresist: Olin 907-12) was used to define the pillar array. Subsequently, the exposed silicon oxide was dry etched (Adixen AMS100DE), after which the resist was removed by oxygen plasma and nitric acid. Another lithography step was then used to define the inlet and outlet channels. The exposed silicon oxide was then re-etched using a Bosch-type deep reactive ion etch (Adixen AMS100SE) was used to make the inlet and outlet channels 60 μm deep. After stripping the resist, another 12 μm was Bosch-etched into the exposed silicon, leaving pillars of 12 μm height and supply channels with a total depth of 72 μm. The channels were subsequently closed off by anodically bonding a 100 mm diameter Pyrex® wafer (thickness 0.5 mm) to the silicon wafer (voltage ramped to a maximum of 1000 V at 400 °C, on an EVG EV-501 wafer bonder). Prior to this, through-holes were defined in the silicon wafer by photolithography using a dry resist foil (Ordyl BF410).

2.2. System hardware and injection procedures

The injection procedure has been described previously and uses an injection zone devoid of pillars preceding the actual pillar channel. This zone defines the injection volume and is connected with the pillar array through a 10 μm wide supply channel followed by a flow distributor region containing transversally oriented diamond shaped pillars which distribute the liquid evenly across the actual cylinder bed (Fig. 2). The size and shape of the band that enters the pillar channel are respectively determined by the injection and distributor zone as fully elaborated in Ref. [22]. A homemade setup containing two pressurized vessels, each controlled by a pressure controller (Bronckhorst, The Netherlands), was used to provide the required pressure for the flow generation in a two-step injection process. The stainless steel vessel containing the mobile phase was coupled to a 0.2 μm pore size filter. The two different pressurized vessels are needed to apply two different independent pressure settings. The sample injection works best at low pressure and needs

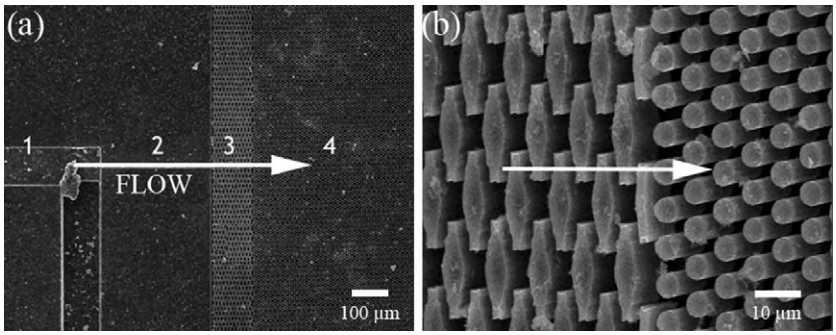

Fig. 2. SEM pictures of the employed micropillar array channel. (a) Taken at the beginning of the micropillar column showing a part of the injection zone (1), the 10 μm wide connection channel (2), the flow distributor (3) and a part of the actual cylindrical pillar bed (4) are shown. (b) A zoom-in of the transition zone between the flow distributor filled with diamond shaped pillars and the actual cylindrical pillar bed.

1.5–3 bar, whereas the mobile phase flow needs a high pressure ranging from 5 to 50 bar. Wide capillaries (i.d. = 150 μm, Achrom, Belgium) were used for the connection between the pressurized vessels and the chip, so that the pressure readout of the pressure controllers could be used as a measure of the pressure at the inlet of the column. Using a homemade program written in C++, the pressure controllers, the external valves (Rheodyne, IDEX, Germany), as well as the translation stage could be simultaneously controlled from one central computer. Linear mobile phase velocities ranging from 0.0075 to 6 mm/s could be generated at working pressures of respectively 1.5 and 45 bar.

For the detection of the fluorescent sample bands, an inverted microscope (IX71, Olympus, Belgium) equipped with a wide green filter cube set was used. Illumination with a Hg-vapor lamp (U-LH100HGAPO, Olympus, Belgium) enabled excitation of fluorescein isothiocyanate (FITC) and the microparticles at 505 nm and emission around 515 nm. The microscope was mounted on a breadboard (M-IG 23–2, Newport, The Netherlands), together with a linear displacement stage (M-TS100DC) and a speed controller (MM, 4006 Newport) used to displace the channels opposite to the movement of the sample bands. The separations were visualized using an air-cooled charge coupled device (CCD) fluorescence camera (ORCA-ER4742, Hamamatsu Photonics, Belgium) mounted on the video adapter of the microscope. Video images were subsequently analyzed with the accompanying SimplePCI 6 software.

2.3. Chemicals

The particles used as test analytes were fluorescently labelled polystyrene latex microparticles (Carboxylate Modified Fluospheres® YellowGreen Fluorescent) of nominal diameters 100, 200 and 500 nm, obtained from Molecular Probes (Leiden, The Netherlands). As specified by the manufacturer, the 100 nm microspheres have a coefficient of variation (CV) of about 5% as determined by electron microscopy, and the size uniformity improves as the size increases (CV down to 1%). FITC sodium salt was obtained from Acros Organics (Geel, Belgium). A sodium tetraborate buffer (3 mM, pH 9.2) with addition of 0.5 g/l Triton X-100 (Acros Organics, Geel, Belgium) is used in all experiments in order to prevent agglomeration of the particles. Solutions of FITC (1×10^{-5} M) and 100, 200 or 500 nm particles (each at a concentration of 0.15% solids) were dissolved in the buffer and sonicated during 10 min before injection.

2.4. Separation procedures

Mixtures of microparticles and FITC were injected at different mobile phase velocities to measure their retention coefficients and their band broadening. Before use, the channels were thoroughly flushed with the aqueous working buffer of pH 9.2 prior to injection. This was done to eliminate undesirable retention caused by interaction with the silicon surface of the channel. In the neutral pH area, adsorption of the negatively charged marker on the partly oxidized silicon surface can occur. To measure the plate heights, the analytes were injected individually and peak variances were monitored at the beginning of the channel and at a given distance downstream in the column. Peak variances were determined either in space or in time, depending on the size of the analyte band. For narrow peaks, the variances could be measured in space. Fluorescence intensity data taken from within a frame of 168 pixels wide and 10 pixels high at the center of the channel were used to generate space-based chromatograms. On the other hand, when peak widths exceeded the width of the recording frame, variances had to be determined in time. A monitorline of 1 pixel wide and 10 pixels high at the center of the channel was used to generate time-based chromatograms. Peak variances were calculated by applying the method of moments on the chromatograms (Eqs. (6) and (7)). Plate heights were subsequently determined using either Eq. (1) (space-based chromatograms) or (2) (time-based chromatograms).

$$H = \frac{\Delta\sigma_x^2}{L} \tag{1}$$

$$H = \frac{U^2\Delta\sigma_t^2}{L} \tag{2}$$

wherein $\Delta\sigma_x^2$ is the difference between the space-based variance of the peak at a position $x = l$ and that at position $x = 0$ (bed entrance), $\Delta\sigma_t^2$ is the difference between the time-based variance of the peak at these positions and U is the mean band velocity. To construct Van Deemter curves, the plate heights were subsequently plotted as a function of the mean mobile phase velocity.

The effective diffusion coefficients for FITC, 100 and 200 nm microparticles in the aqueous buffer were measured by performing so-called peak parking experiments [23–25]. In such an experiment, the column flow is stopped as soon as a peak has reached a given position in the column. Peak variances of the continuously broadening arrested peak are subsequently monitored over a given time interval. Effective diffusion coefficients can subsequently be calculated using Eq. (3) [26].

$$\Delta\sigma_x^2 = 2D_{\text{eff}}\Delta t \tag{3}$$

wherein $\Delta\sigma_x^2$ is the difference between the space-based variance of the arrested peak at different time intervals.

3. Results and discussion

3.1. Determination of D_{mol} and D_{eff}

Effective diffusion coefficients (D_{eff}) were determined for FITC, 100 and 200 nm particles by means of peak parking experiments. Continuously monitoring the bands with the CCD-camera allowed to verify that the bands did not move during the peak parking, so that only diffusion contributed to the observed peak broadening. Since the molecular diffusion coefficient for FITC has been calculated in earlier work [27], the obstruction factor γ of the pillar array bed could be calculated according to Eq. (4). The value for γ was found to be 0.588 ± 0.006. According to Computational Fluid Dynamics (CFD) simulations done in our group, a micropillar array with an external porosity ε of 0.4 can be expected to have a γ value of 0.62 [28]. It is believed that this small discrepancy between experiment and theory can be attributed to the occurrence of some reversible adsorption of the particles onto the channel walls, slowing down the diffusion process.

$$D_{\text{eff}} = \gamma D_{\text{mol}} \tag{4}$$

In order to compare theoretical and experimental values for the D_{eff}-values measured for the microparticles, D_{mol}-values for the microparticles were calculated using the Stokes–Einstein equation and multiplied by the γ-factor found for FITC.

$$D_{\text{mol}} = \frac{kT}{6\pi\eta r} \tag{5}$$

wherein k is the Boltzmann constant, T is the absolute temperature in Kelvin, η is the viscosity and r is the radius of the particles. Fig. 3 shows the peak variances of 3 subsequent FITC injections as a function of the elapsed time. For small molecules like FITC, the data could be acquired in a relatively short period, while for larger particles the variances had to be monitored during a longer period in order to obtain representative results.

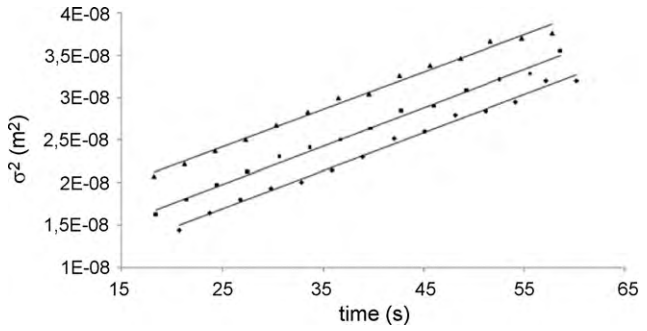

Fig. 3. Plot of band variance as a function of the time for 3 different peak parking experiments with FITC (the difference between the curves is due to difference in applied injection volume). The slopes for the 3 curves are from top to bottom 4.49×10^{-10}, 4.53×10^{-10} and 4.45×10^{-10} m^2/s with respectively R^2 values of 0.9916, 0.9949 and 0.9933.

Table 1
Experimental and theoretical values for D_{eff} of FITC, 100, 200 and 500 nm particles.

	D_{eff}	
	Experiment[a,c]	Theory[b]
FITC	$2.25 \times 10^{-10} \pm 2.13 \times 10^{-12}$	
100 nm	$2.36 \times 10^{-12} \pm 2.37 \times 10^{-13}$	2.52×10^{-12}
200 nm	$1.04 \times 10^{-12} \pm 2.12 \times 10^{-13}$	1.26×10^{-12}
500 nm	$5.09 \times 10^{-13} \pm 3.36 \times 10^{-14}$	5.05×10^{-13}

All diffusion coefficients are given in m^2/s.
[a] Calculated using Eq. (3).
[b] Calculated using Eqs. (4) and (5).
[c] Mean ± SD, $n = 3$.

Table 1 lists the theoretical and experimental diffusion coefficients for FITC and the different microparticles. For the finite size solid particles, the theoretical diffusion coefficient was calculated from Eq. (5). It can be remarked that the experimental values for the

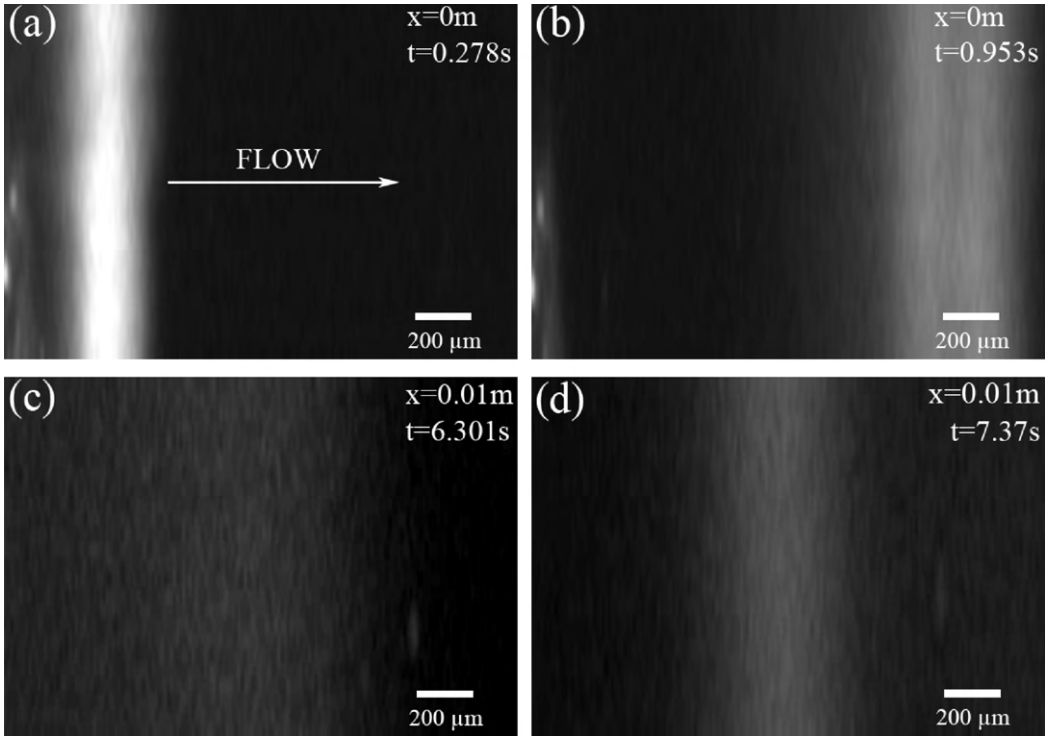

Fig. 4. CCD-camera images of the injection and migration of a mixture of FITC and 100 nm particles in the micropillar array. (a and b) Images recorded at a position immediately after the injection slit (a: at $t = 0.278$ s; b: $t = 0.953$ s). (c and d) Images recorded at a position 0.01 m downstream the injection slit (c: 100 nm particle band; d: FITC band). Mobile phase = 3 mM sodium tetraborate, 0.5 g/l Triton X-100, pH 9.2. Mobile phase velocity = 1.4 mm/s. Mobile phase inlet pressure = 25 bar and sample inlet pressure = 2 bar.

effective diffusion coefficients are systematically lower than what the theory predicts. Again, this deviation probably can be attributed to the fact that the particles are likely to adsorb onto the pillar surface, leading to lower values for D_{eff}.

3.2. Determination of relative retention times

An example of a typical separation experiment is shown in Fig. 4. Mixtures of FITC and microparticles were injected to investigate the hydrodynamic separation performance of the micropillar array. Within seconds after the injection, the separation already becomes apparent. Although the sample clearly enters the channel as a single fluorescent band (Fig. 4a) two distinct bands (the first being the 100 nm particles and the latter FITC) can already be observed in a video frame taken some 0.6 s later at the same recording position (Fig. 4b). The faster elution of the 100 nm particles is in accordance with the HDC theory, where analytes with a larger hydrodynamic radius experience a higher overall velocity and elute according to their size, with the largest eluting first. At a position 1 cm downstream in the channel, the distance between the bands had grown to that extent that visualization of both bands in one picture became impossible. Fig. 4c shows the 100 nm particle band, whereas Fig. 4d shows the FITC band eluting about 1 s later. Moving the camera with a computer driven translation table allowed the precise monitoring of the speed of the migrating bands throughout the whole column.

When a mixture containing all analytes was injected, the larger particles obviously travelled at a higher mean velocity as compared to the smaller ones. However, the bands showed substantial overlapping, making quantitative analysis of these separations impossible. Hence, relative elution times were determined by injecting each particle size separately with respect to FITC. But even for these binary mixtures, a complete baseline separation could not readily be obtained, as can be seen in Fig. 5a. Whereas the FITC bands very rapidly assumed a Gaussian distribution when travelling through the column, time, the peak profiles of the particles did not have a Gaussian distribution. This forced us to reconstruct a small part of the peak to determine the residence time according to the method of moments (Fig. 5b). For the reconstruction of the

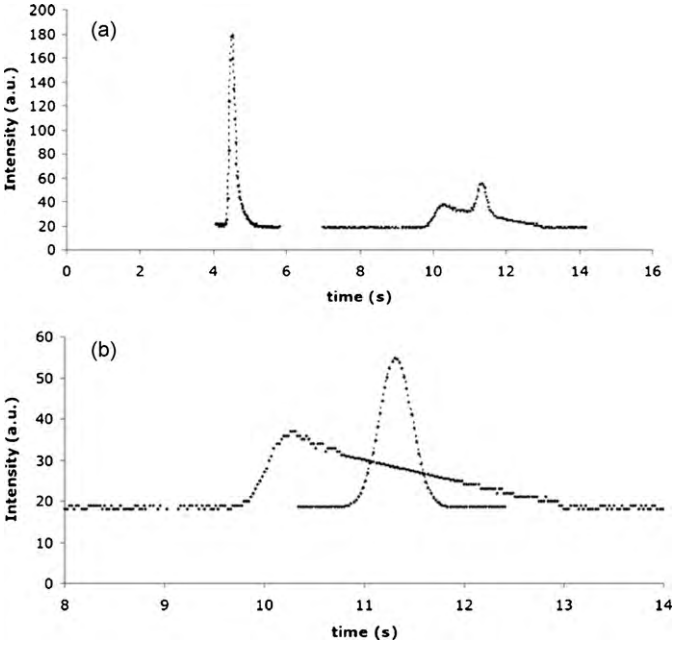

Fig. 5. Intensity readouts generated from the source movie clip from which the images in Fig. 4 were generated. (a) Chromatograms recorded at 0 and 1 cm downstream the column. (b) Close-up of the chromatogram recorded 1 cm downstream the column, showing the result of the reconstruction approach described in the text.

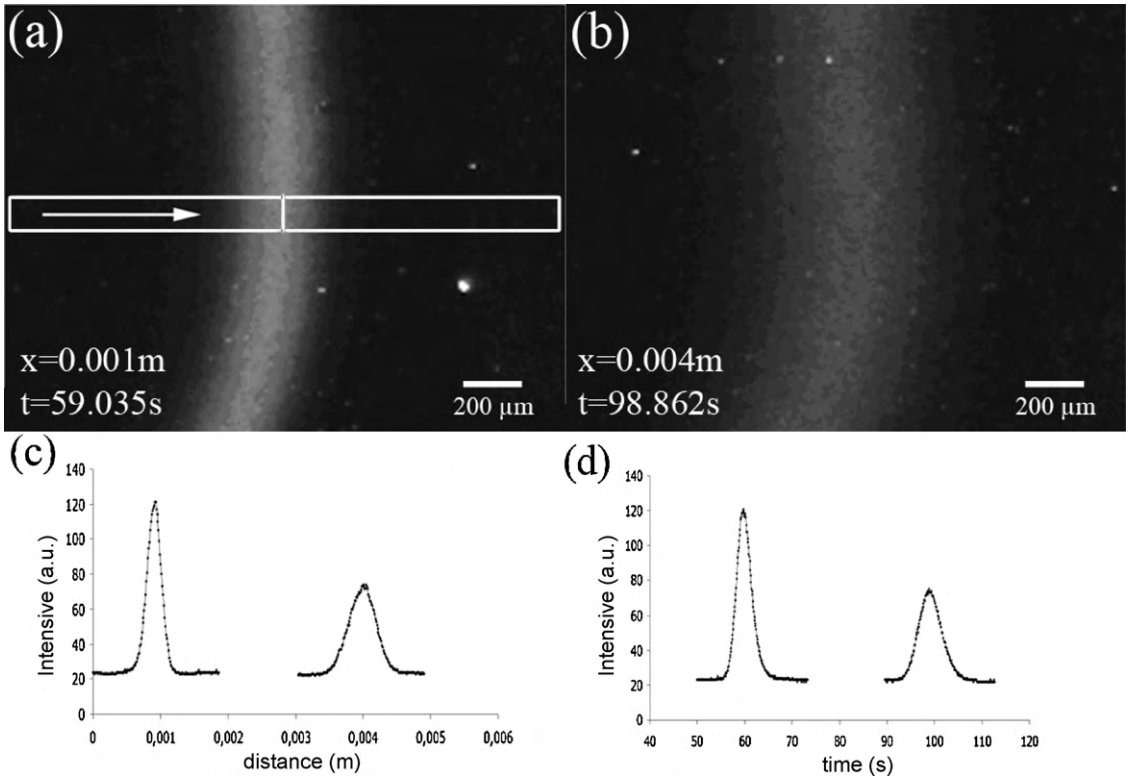

Fig. 6. CCD images of fluorescent 100 nm particle bands taken at respectively 1 and 4 mm downstream the injection zone (a and b). The frame (shown in panel a) was 168 pixels wide and 10 pixels high and the monitorline was 1 pixel wide and 10 pixels. Intensity readout as a function of space (c) and as a function of time (d). Mobile phase = 3 mM sodium borate, 0.5 g/l Triton X-100, pH 9.2. Mobile phase velocity = 0.07 mm/s. Mobile phase inlet pressure = 5 bar and sample inlet pressure = 2 bar.

Table 2
Relative retention measured 1 cm downstream the injection zone.

	τ	
	Experimental	Theory
Particles		
100 nm	0.951 ± 0.003	0.96
200 nm	0.925 ± 0.004	0.93
500 nm	0.905 ± 0.004	0.86

τ values were determined in relation to FITC; mean values ± SD; $n = 3$; measured at different mobile phase velocities.

peaks, a Gauss function was fitted through the baseline and the apex of the FITC peak. After this reconstruction, a separate peak profile is obtained for the FITC and the particles. The latter peak could subsequently be integrated using the method of moments. It is believed the peaks are reconstructed without significantly affecting their width. The elution time at which the mean of the peak passes the monitorline was then obtained by dividing the first statistical moment m_1 by the zeroeth moment m_0 (Eqs. (6) and (7)). Residence times for the peaks in Fig. 5b were $t = 10.97$ s for the 100 nm particles and 11.31 s for FITC. The relative retention factor τ calculated from this data is hence (10.97 s − 4.57 s)/(11.31 s − 4.57 s) = 0.95. The second moment m_2 is calculated in order to determine the variance of the peaks (Eq. (8)).

$$m_0 = \int_0^{+\infty} I \, dt \tag{6}$$

$$m_1 = \frac{1}{m_0} \int_0^{+\infty} tI \, dt \tag{7}$$

$$m_2 = \int_0^{+\infty} (t - m_1)^2 I \, dt \tag{8}$$

Table 2 shows the experimental values for the relative retention time of the different microparticles as compared to FITC. The linear velocity of FITC bands was used as a measure of mobile phase velocity because the homemade setup did not allow precise monitoring of the flow through the columns. The retention behaviour of microparticles in the case of flat-rectangular channels can be accurately described by the model developed by Di Marzio and Guttman for a system of plane parallel plates [4]. In this model, the relative retention time depends solely on the relative size of the analyte with respect to the flow channel (Eq. (9)). Even though this model does not account for additional effects occurring when spherical particles move through the pillar bed array (Hydrodynamic interaction, tubular pinch) [29,30], the theoretical predictions according to this model seem to be fairly in accordance with the experimental values obtained in the present study. In this case we used the actual interpillar distance (2.5 μm) as the size of the flow channel in the definition of λ ($\lambda = d_{particle}/d_{interpillar}$) In reality the flow-through channels are larger, resulting in a smaller value for λ and thus a slightly altered theoretical value for τ.

$$\tau = (1 + \lambda - \lambda^2)^{-1} \tag{9}$$

3.3. Determination of plate heights as a function of u

In order to measure experimental plate height values, peak variances were monitored either in space or in time. We demonstrate this in Fig. 6. The peak variances were 1.10×10^{-8} and 3.34×10^{-8} m^2 at 1 and 4 mm respectively when measuring in space and 1.81 and 5.38 s^2 when measuring in time. Theoretical plate heights of 7.35 and 7.13 μm respectively were obtained. The small discrepancy between both values is probably due to small peak fitting errors, as the peaks are not perfectly symmetrical.

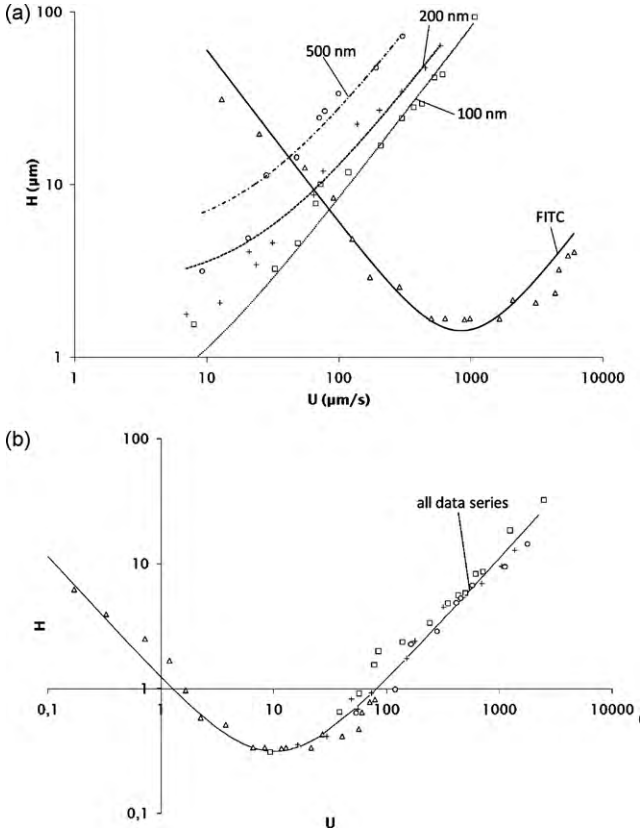

Fig. 7. Superposition of the normal (a) and the reduced (b) Van Deemter curves of FITC (△), 100 nm (□), 200 nm (+) and 500 nm (○) fluorescent microspheres. The full line represents the best fitted curve according to the reduced Van Deemter equation (Eq. (12)) ($A = 0.09$, $B = 1.13$, $C = 0.01$).

To characterize band broadening properties of the pillar array used in the present study, a Van Deemter curve was first established for FITC (Fig. 7). Minimal plate heights in the order of 1.6 μm were obtained, which is in accordance with earlier non-retained species experiments conducted in pillar array columns [17,19,20]. In the same graph we present the Van Deemter curves for the different microparticles. The measured minimal plate heights of FITC and the 100 nm particles have the same order of magnitude (i.e. around 1.6 μm). As the optimal mobile phase velocity was not reached for the 200 and 500 nm particles, the minimal plate height value could not be reached. As theoretically expected, the minima shift towards smaller mobile phase velocities as the size of the particles increases. Using the effective diffusion coefficients for the different analytes and the pillar diameter, plate heights and mobile phase velocities can be made dimensionless (Eqs. (10) and (11)).

$$\nu = \frac{Ud}{D_{mol}} \tag{10}$$

$$h = \frac{H}{d} \tag{11}$$

$$h = A + \frac{B}{\nu} + C\nu \tag{12}$$

As seen in Fig. 7b, experimental Van Deemter curves for the different analytes more or less follow a similar course when reduced, with minimal plate heights around 0.3. The experimental values were fitted to the Van Deemter equation (Eq. (12)) and the result is represented by the whole line in the graph (fitting parameters

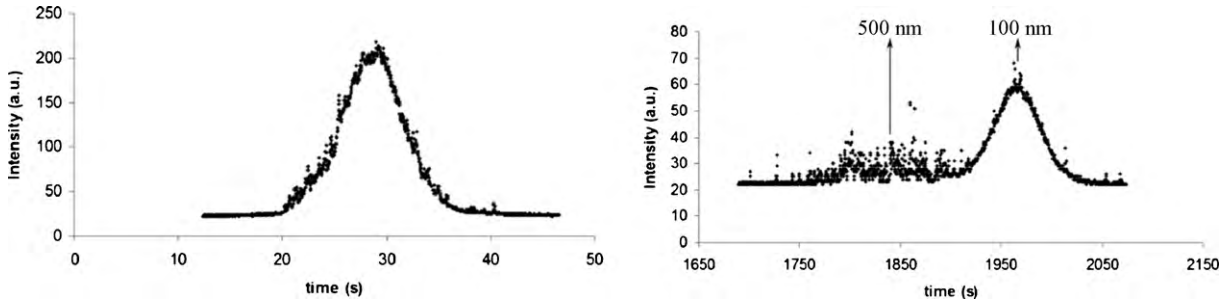

Fig. 8. Time-resolved chromatograms of a mixture of 100 and 500 nm microparticles. Peaks are monitored at the beginning (x = 0 cm) (a) and at the end (x = 2.5 cm) (b) of the column.

are given in the capture to Fig. 7). Striking to note is the extremely small C-term constant (C = 0.01, i.e. much smaller than in a random packed-bed column, where usually C = 0.05–0.1) [31]. Also the A-term constant is extremely low (A = 0.09), reflecting the increased order, and hence the reduced Eddy-dispersion of a pillar array column as compared to a packed-bed column, where typically A = 0.5–1. The fitting lines in Fig. 7a were derived from the same equation using Eqs. (10) and (11) to back transform the data in the H, U-format.

3.4. Some separation results

Because the minimal obtainable plate heights, retention coefficients and the column length are all known, the separation resolution between the studied analytes can be calculated according to Eq. (13). The minimum separation resolution needed before two components can be considered to be sufficiently separated, is generally agreed to be given by R_s = 1.5. As seen in the series of preliminary separation experiments we conducted in the present study, the pillar array used in this study does not confer sufficient resolution to separate all 4 components. However, the column length needed to achieve significant resolution can be calculated by combining Eqs. (2), (13) and (14), which results in Eq. (15). As the maximum separation efficiency is achieved at different mobile phase velocities for analytes of a different size, a compromise has to be made regarding this velocity. The highest resolution can be achieved at the mobile phase velocity for which the average of both plate heights is at its minimum. For the separation of 100, 200 and 500 nm particles, this velocity was found to be 8.5 μm/s. Theoretical calculations confirmed our experimental findings that a 2.5 cm long column was not long enough to separate 100 and 200 nm microparticles. The minimal column length needed for this separation was found to be about 10 cm. When these calculations were made for 100 and 500 nm microparticles, the minimal column length needed to achieve R_s = 1.5 was found to be about 3.9 cm. So again our column length appeared to be insufficient. Nonetheless, reasonable separations should already be possible in the 2.5 cm column length we had at our disposition. To demonstrate this, a mixture of 100 and 500 nm microparticles was monitored while travelling through the column at a mobile phase velocity of 12 μm/s. Chromatograms were recorded at the beginning and the end of the column (Fig. 8).

$$R_s = \frac{t_0 \Delta\tau}{4\sigma_t} \tag{13}$$

$$\sigma_t = \frac{\sigma_x}{U} = \frac{\sqrt{HL}}{U} \tag{14}$$

$$L = \left(\frac{4R_s}{\Delta\tau}\right)^2 H \tag{15}$$

In Fig. 8a, a chromatogram recorded at the beginning of the column reveals one peak ($\sigma_t^2 = 9.3\,s^2$) containing both types of particles. As compared to chromatograms in Figs. 5 and 6, the course of the curve is rather rough. This is due to the fact that 500 nm particles are no longer seen as a continuous band (as the FITC and the 100 and 200 nm particles). Instead, the particles appear as discrete features. Fig. 8b shows a chromatogram recorded at the end of the column, in which it is possible to distinguish between the 100 and 500 nm particles. Whereas the first size leads to a smooth peak profile, the second size leads to a rather rough collection of discrete points. At a mobile phase speed of 12 μm/s, plate heights as low as 1.8 and 3.3 μm could be obtained for respectively the 100 and the 500 nm particles (smooth peak, $\sigma_s^2 = 320.2\,s^2$) Even though the separation is already apparent in the chromatograms, a complete separation resolution has not yet been reached for this separation. An average plate height of 2.6 μm and a selectivity of 0.046 can be expected to result in a separation resolution of only 1.1 at 2.5 cm.

4. Conclusions

Testing the HDC separation properties of a micropillar array column, the experimental selectivity (expressed in term of τ as a function of λ) for hydrodynamic separations was found to be more or less similar to the on-chip HDC system of Chmela et al. [13] and to that obtained in a recent study where hydrodynamic chromatography of silica colloids was performed on packed-bed columns [32]. However, the minimal obtainable reduced plate height for the micropillar array was much lower than 1 (h = 0.3), so that the micropillar array format can be considered promising for the implementation of hydrodynamic chromatography. A next series of experiments is now planned using chips with longer channels to achieve better resolution of the band.

Nomenclature

A	constant in Eq. (12) for Eddy diffusion (/)
B	constant in Eq. (12) for longitudinal diffusion (/)
C	constant in Eq. (12) for mass transfer resistance (/)
d	pillar diameter (m)
D_{eff}	effective diffusion coefficient (m^2/s)
D_{mol}	molecular diffusion coefficient (m^2/s)
h	reduced height equivalent of a theoretical plate (/)
H	height equivalent of a theoretical plate (m)
I	fluorescence intensity (arbitrary units)
k	Bolzmann constant (J/K)
L	column length (m)
m_0	zeroeth statistical moment (s)
m_1	first statistical moment (s^2)
m_2	second statistical moment (s^3)
R_s	resolution (/)
r	sphere radius (m)
T	absolute temperature (K)

t_0 residence time of unretained marker (FITC) (s)
U mobile phase linear velocity (m/s)

Greek letters
γ obstruction factor (/)
ε interstitial porosity (/)
η dynamic mobile phase viscosity (kg/(m s))
λ relative analyte size (/)
λ reduced mobile phase linear velocity (/)
σ_t^2 variance in t direction of the concentration peak (s^2)
σ_x^2 variance in x direction of the concentration peak (m^2)
τ relative retention time (/)

References

[1] H. Small, M. Langhorst, Anal. Chem. 54 (1982) 892A.
[2] E. Venema, J.C. Kraak, H. Poppe, R. Tijssen, J. Chromatogr. A 740 (1996) 159.
[3] A. Williams, e. Varela, E. Meehan, K. Tribe, Int. J. Pharm. 242 (2002) 295.
[4] E.A. Di Marzio, C.M. Guttman, Macromolecules 3 (1970) 131.
[5] J.C. Giddings, J. Sep. Sci. 1 (1966) 123.
[6] J. Janca, Int. J. Polym. Anal. Charact. 11 (2006) 57.
[7] T.L. Edwards, B.K. Gale, A.B. Frazier, Anal. Chem. 74 (2002) 1211.
[8] D. Kang, M.H. Moon, Anal. Chem. 77 (2005) 4207.
[9] M. Yamada, M. Seki, Lab Chip 5 (2005) 1233.
[10] D. Huh, J.H. Bahng, Y. Ling, H.H. Wei, O.D. Kripfgans, J.B. Fowlkes, J.B. Grotberg, S. Takayama, Anal. Chem. 79 (2007) 1369.
[11] R. Tijssen, J. Bos, M.E. van Kreveld, Anal. Chem. 58 (1986) 3036.
[12] J. Bos, R. Tijssen, J. Chromatogr. Libr. 56 (1995) 95.
[13] E. Chmela, R. Tijssen, M. Blom, Anal. Chem. 74 (2002) 3470.
[14] M.T. Blom, E. Chmela, J.G.E. Gardeniers, Sens. Actuators B 82 (2002) 111.
[15] M.T. Blom, E. Chmela, R.E. Oosterbroek, R. Tijssen, A. Van den Berg, Anal. Chem. 75 (2003) 6761.
[16] N. Vervoort, J. Billen, P. Gzil, G. Baron, G. Desmet, Anal. Chem. 76 (2004) 4501.
[17] W. De Malsche, H. Eghbali, D. Clicq, J. Vangelooven, H. Gardeniers, G. Desmet, Anal. Chem. 79 (2007) 5915.
[18] M. De Pra, W. De Malsche, G. Desmet, P.J. Schoenmakers, W.T. Kok, J. Sep. Sci. 30 (2007) 1453.
[19] H. Eghbali, W. De Malsche, D. Clicq, H. Gardeniers, G. Desmet, LC–GC Eur. 4 (2007) 208.
[20] M. De Pra, W.Th. Kok, J.G.E. Gardeniers, G. Desmet, S. Eeltink, J.W. van Nieuwkasteele, P.J. Schoenmakers, Anal. Chem. 78 (2006) 6519.
[21] W. De Malsche, D. Clicq, V. Verdoold, P. Gzil, G. Desmet, H. Gardeniers, Lab Chip 7 (2007) 1705.
[22] J. Vangelooven, W. De Malsche, J. Op De Beeck, H. Eghbali, H. Gardeniers, G. Desmet, Lab Chip 10 (2010) 349.
[23] H. Kobayashi, D. Tokuda, J. Ichimaru, T. Ikegami, K. Miyabe, N. Tanaka, J. Chromatogr. A 1109 (2006) 2.
[24] K. Miyabe, Y. Matsumato, G. Guiochon, Anal. Chem. 79 (2007) 1970.
[25] F. Gritti, G. Guiochon, Chem. Eng. Sci. 61 (2006) 7636.
[26] J.C. Giddings, Dynamics of Chromatography Part 1, Marcel Dekker, New York, 1965.
[27] K. Pappaert, Ph.D. Thesis, Vrije Universiteit Brussel, Brussels, Belgium, 2005.
[28] G. Desmet, K. Broeckhoven, J. De Smet, S. Deridder, G.V. Baron, P. Gzil, J. Chromatogr. A 1188 (2008) 171.
[29] H. Brenner, L.J. Gaydos, J. Colloid Interface Sci. 58 (1977) 312.
[30] H.J. Ploehn, Int. J. Multiphase Flow 13 (1987) 773.
[31] P.A. Bristow, J.H. Knox, Chromatographia 10 (1977) 279.
[32] T. Takeuchi, Siswoyo, Z. Aspanut, L.W. Lim, Anal. Sci. 25 (2009) 301.